Limitations of accuracy in PIV due to individual variations of particle image intensities

H Nobach and E Bodenschatz

February 6, 2007

Max Planck Institute for Dynamics and Self-Organization, Göttingen, Germany

Abstract

The effect of individual tracer particle intensity variations in consecutive images on the accuracy of the displacement estimates in particle image velocimetry is investigated. Particularly, the efficacy of Gaussian low-pass filter image interpolation for the reduction of under-sampling, the normalization of the correlation estimates for reduction of truncation errors, and interrogation area weighting schemes for improved spatial resolution are studied. The achievable accuracy of PIV measurements is shown to be limited by this effect to approximately 0.1 pixels.

1 Introduction

Particle image velocimetry (PIV) has become the prime choice for processing image-based flow measurements in fluid dynamics experiments. The basic algorithm of digital PIV processing [1, 2, 3, 4], utilizes the cross-correlation of image sub-spaces for local displacement estimation from two consecutively acquired images of a particle-laden flow field. During the last years PIV has been improved by increasing both, the attainable accuracy of velocity estimates and the spatial resolution [5].

Using appropriate sub-pixel interpolation of the correlation planes, the achievable accuracy of the measurement of the particle displacement can be significantly improved over the nominal resolution of the optical sensor. Widely used in PIV are the peak centroid (center-of-mass) method [6, 7] and the Gaussian interpolation [2]. The remaining systematic error of the displacement estimate is periodic with respect to the discrete resolution of the sensor, yielding the "pixel locking" or "peak locking" [8, 9, 10, 11, 12] and limits the achievable accuracy.

An additional error occurs due to the edges of the interrogation areas, where particle images are truncated. This error has been identified as an accuracy-limiting factor [13]. The normalization of the correlation values with individual estimates of the image intensity variance [2, 14, 15, 10, 17] has been found to be an efficient correction method [16, 18].

A further improvement can be achieved by iteratively applying window-shift and window-deformation techniques [19, 20, 5], or image deformation [21, 22]. These techniques iteratively optimize the estimated velocity field towards vanishing displacements between image sub-spaces, which are shifted and deformed accordingly to the assumed velocity field. Because of the vanishing displacement, the results are almost independent of the utilized correlation plane sub-pixel interpolation scheme (correlation peak centered around zero) and of particle image truncations at the edges of the interrogation area (similar patterns in both interrogation areas are correlated). Nevertheless, the shifted and deformed image sub-spaces are obtained by re-sampling the original images at appropriate sub-pixel position. Thus, an appropriate image sub-pixel interpolation is required.

Since the accuracy of the velocity estimates directly depends on the quality of the image interpolation, the simple, but widely used, bi-linear interpolation yields poor results. Higher-order interpolation schemes have been shown to be advantageous [9, 23, 24, 25, 26]. In particular, bi-cubic splines and the Whittaker interpolation [27] (also known as sinc or cardinal interpolation) have found wide acceptance. Recently, a Gaussian low-pass filter for image interpolation and re-sampling was introduced [28] to further improve the accuracy by reducing the system-inherent under-sampling of the particle images.

Since the correlation of image sub-spaces implicitly averages the displacement information over the interrogation areas, the achievable accuracy of uniformly displaced particle image patterns does not sufficiently reflect the quality of the estimation in a flow field with varying velocity. The question of the ability to resolve velocity fluctuations has become of major interest during the last few years [29]. The spacial resolution of the iterative window shift and deformation techniques is fundamentally limited by the the size of the interrogation areas. Iterative image deformation techniques can improve the situation with a high degree of freedom in the deformation of the interrogation areas, by applying a relatively high overlapping of neighboring interrogation areas. In this case, the usual correlation of rectangular interrogation areas has a significant instability at certain spatial frequencies [30, 31, 32]. Therefore, an appropriate low-pass filtering of the velocity data is necessary. Unfortunately, this again substantially limits the spatial resolution. A promising alternative is given by applying a certain weighting to the interrogation areas, which yields only positive values of the frequency response function in the entire range of spatial frequencies [30, 31, 33, 34].

All three techniques (Gaussian interpolation, normalization and interrogation area weighting) have been shown to work to high accuracy. In studies based on synthetic images an accuracy of the order of 0.01 pixel has been reported [20]. In contrast, the application to real images from experiments shows less optimistic results, where the usually observed limit is of about 0.1 pixel. Only under special conditions, like in two-dimensional flows with carefully aligned laser sheets, a better accuracy has been achieved [35].

A possible reason for the different achievable accuracy in simulations and experiments may be the fact that in experiments, particles usually change their

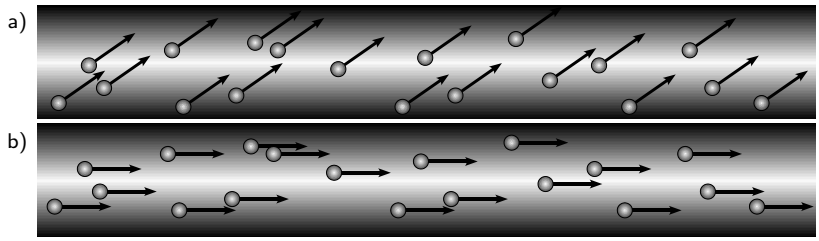

Figure 1: Particles moving in a laser sheet with an intensity profile: a) with an out-of-plane component (all components may have gradients) and b) a two-dimensional flow aligned with the laser sheet plane (only in-plane components may have gradients, out-of plane component must be zero)

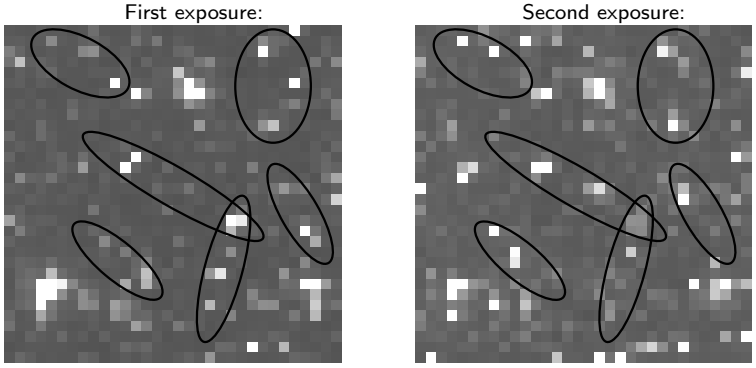

Figure 2: Example for individual particle intensity variations (detail of public PIV images from the PIV challenge 2003, case A, axisymmetric turbulent jet in stagnant surrounding, images A001a and A001b, marked regions with examples of individual particle intensity variations)

position within the laser sheet (figure 1a). Therefore, the particles are illuminated differently in the two consecutive exposures. Additionally, the different illumination is individually different for each particle due to their different starting positions perpendicular to the light sheet plane, even if there is no gradient of the out-of-plane velocity component. The result is an individual variation of particle intensities. The same effect occurs if the two consecutive light sheets are misaligned.

Simulations often assume individual intensities for each particle, but identical intensities in the two exposures, as it can be realized in experiments only in two-dimensional flows with laser sheets exactly aligned parallel to the flow field (figure 1b). On the other hand, individual intensity variations can be easily seen in images from a variety of PIV applications, where some particles become brighter between the two exposures, whereas other particles, even close by, become darker (figure 2).

The possible precision of the basic PIV processing technique with window shift and deformation and the three above mentioned extensions are verified under the condition of varying particle image intensities. To keep the investigations clear and simple and to isolate the effect of individual variations of particle image intensities, the PIV process has been simulated in this study. Except for the intensity variations, all other conditions are ideal, namely here only the case of uniform velocity is investigated with sampled Gaussian-like particle intensity profiles without noise or background gray level. The conclusions are equally applicable to the case of velocity fields with gradients. In that case, however, other well known effects, like limited spatial resolution may additionally influence the results. Errors due to the diffraction-limited imaging or integration over the sensor areas also superimpose.

Note that the case with a variation of individual particle image intensities is different from the loss-of-pairs and from the degradation of the correlation peak due to the out-of-plane motion [36, 3, 37, 38] or illumination variations [15]. On the one hand, the loss-of-pairs increases the sensitivity to noise and the probability of outliers, and occurs additionally to the here discussed effect. On the other hand, the illumination variation can be corrected with appropriate image pre-processing techniques, while the here shown effect cannot. Nonetheless, image generation procedures that consider the out-of-plane motion of particles in a laser sheet with an intensity-varied profile are able to simulate such conditions and the shown effect.

2 Effect of varying intensities

In PIV the displacement of particle patterns between consecutive images is obtained from the peak position in the two-dimensional cross-correlation plane of the two images. Assuming (i) a certain number of imaged particles in the interrogation area, each with different intensity, but with the same relative intensity in the two consecutive images and (ii) no truncation at the edges of the interrogation areas, the correlation peak is at the correct position, even if the

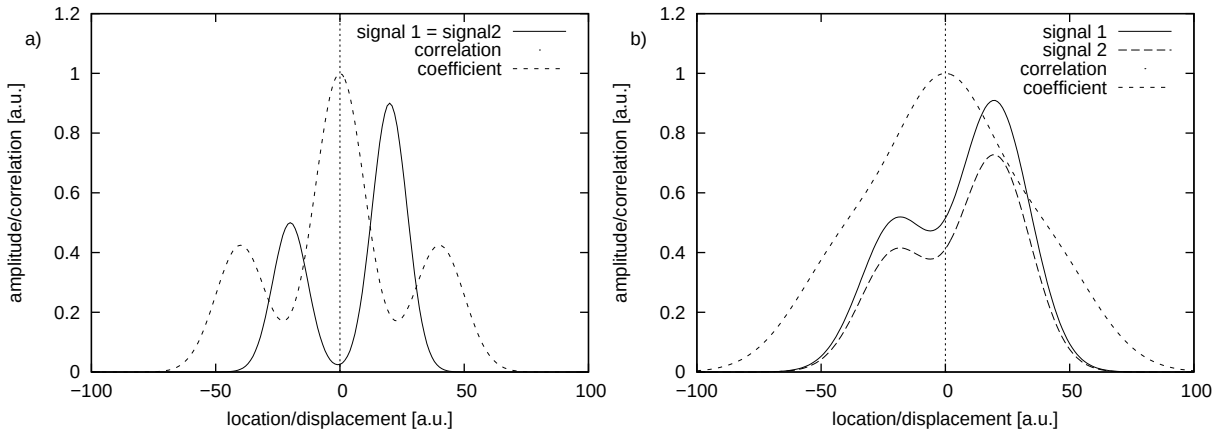

Figure 3: Intensity and cross-correlation function of two signals, each consisting of two peaks with Gaussian intensity profiles: a) same intensity of the profiles in the two signals with well separated peaks and b) one signal scaled and with overlapping peaks

particle images overlap and if the intensity of one entire image is scaled by a constant factor. For demonstration, in figure 3 two signals, each consisting of two well separated peaks with Gaussian intensity profiles are correlated. The peaks are at identical positions in the two signals (no displacement between the signals). The correct position of the correlation maximum at zero displacement can be seen clearly even for overlapping intensity profiles and also with a constant scaling of one signal (figure 3b).

This holds true also for the correlation of Gaussian intensity profiles with different amplitudes[1], as long as the intensity profiles do not overlap in the individual signals (figure 4a). With overlapping intensity profiles of varying amplitude (figure 4b), the maximum position of the correlation peak is clearly shifted, yielding a biased displacement estimate depending on the amplitudes of the intensity profiles, widths and overlap.

The consequence for PIV image processing is an additional error of displacement estimates, if the intensities of particle images vary between the consecutive PIV images, while the particle images overlap. This error is especially large in densely seeded flows or de-focussed images (where the particle images tend to overlap) and in the case of misaligned laser sheets or flows with an out-of-plane motion of the particles (where the illumination of individual particles changes between the two light pulses).

[1]Such variations of the intensity are typical for misaligned light sheets or particles moving out-of-plane, located at different intensity slopes of the light sheet profile

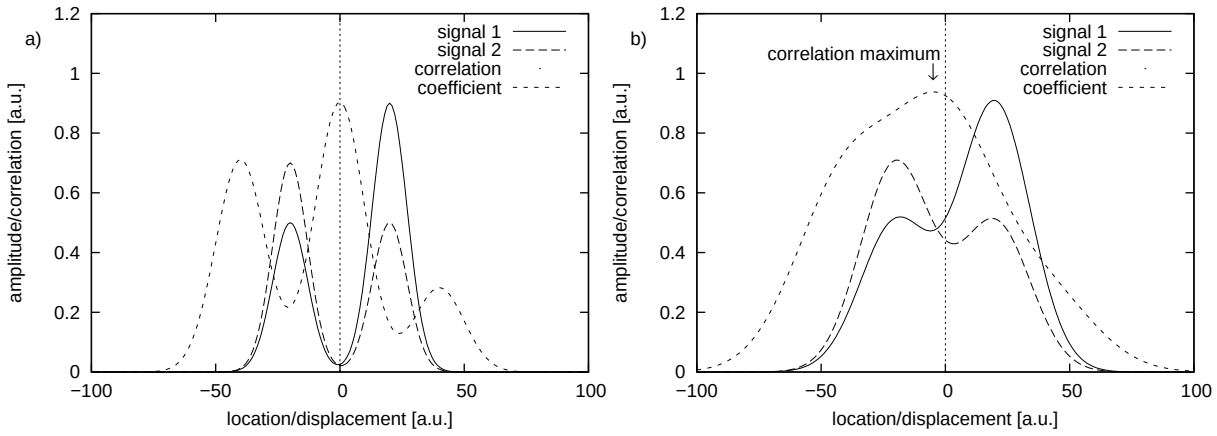

Figure 4: Intensity and cross-correlation function of two signals, each consisting of two peaks with Gaussian intensity profiles: a) varying relative intensity of well separated peaks and b) varying relative intensity of overlapping peaks yielding a correlation peak with a shifted maximum location

3 Image generation

The simulated particle images are two-dimensional Gaussian functions sampled at the center positions of the pixels (diameter given by e^{-2} of the maximum (center) intensity). Neither diffraction-limited imaging nor intensity integration over the sensor areas have been considered here to keep the investigation as simple as possible and to isolate the investigated effect of individual particle intensity variations. The particles are uniformly distributed over the observation area. The simulated displacement of the particles between the two exposures is randomly chosen between -1 and $+1$ pixels, but constant for all particles, simulating a homogeneous velocity field. Overlapping particle images are superimposed linearly. The maximum intensities of the consecutive particle images I_A and I_B are calculated for each simulated particle independently from a double random process using $I_\mathrm{A} = \zeta_0\zeta_\mathrm{A}$ and $I_\mathrm{B} = \zeta_0\zeta_\mathrm{B}$ with the uniformly distributed random values ζ_0, ζ_A and ζ_B between zero and unity. This simulates the correlation between the intensities in the consecutive images due to the constant particle size and the different illumination of this particle by the two exposures. To keep the investigation as simple as possible and to isolate the investigated effect of individual particle intensity variations, no noise or background gray value have been added.

4 Image processing

Modern PIV algorithms with iterative window shift and window deformation techniques [19, 20, 5] or image deformation [21, 22] make use of a sub-pixel re-

sampling of the consecutive images based on pre-estimates of the velocity field. in this study, the simulated images are interpolated and re-sampled, either with a random pre-estimate of the displacement (uniformly distributed between -1 and $+1$ pixels) or assuming the correct displacement from simulation as the pre-estimate, which, in the ideal case, is asymptotically approached by an iterative correction loop. A bi-linear interpolation has been used for reference, while a bi-cubic spline interpolation, a Whittaker interpolation and a Gaussian low-pass filter [28], all based on a 8×8 pixel image sub-space, have been used for comparison.

The interpolated and re-sampled interrogation areas $f(i;j)$ and $g(i;j)$ with a size of 48×48 pixels ($i;j \in [0 \ldots 47]$) are cross-correlated using FFT routines assuming periodic boundaries yielding

$$R(k;l) = \sum_{i;j=0}^{47} f(i;j)g(i+k;j+l) \tag{1}$$

where $f(i+I \times 48; j+J \times 48) = f(i;j)$ and $g(i+I \times 48; j+J \times 48) = g(i;j)$ with $i;j \in [0 \ldots 47]$ and $I;J \in \mathbb{Z}$ or using the normalized correlation coefficient (without periodic boundaries)

$$\rho(k;l) = \frac{\sum_{i;j=0}^{47} f(i;j)g(i+k;j+l)}{\sqrt{\left(\sum_{i;j=0}^{47} f^2(i;j)\right)\left(\sum_{i;j=0}^{47} g^2(i+k;j+l)\right)}} \tag{2}$$

where $f(i;j)$ and $g(i;j)$ are zero outside the interrogation area ($f(i;j) = g(i;j) \equiv 0 \; \forall \; i;j \notin [0 \ldots 47]$).

In the case of using interrogation area weighting schemes [30], the image data $f(i;j)$ and $g(i;j)$ in equation 1 are replaced by the weighted image data $w(i;j)f(i;j)$ and $w(i;j)g(i;j)$ yielding

$$R(k;l) = \sum_{i;j=0}^{47} w(i;j)f(i;j)w(i+k;j+l)g(i+k;j+l) \tag{3}$$

where $w(i;j)$ is a two-dimensional triangular function

$$w(i;j) = \left[1 - \left|\frac{i-23.5}{24}\right|\right]\left[1 - \left|\frac{j-23.5}{24}\right|\right] \tag{4}$$

Note that this weighting function is similar (except for the different scaling, which is non-relevant for the functionality) to the recommendation in [30], where $w^2(i;j)$ has been defined instead. For the weighted correlation coefficient with normalization the "doubled weighting" from [34] has been used with averaging of the correlation coefficients yielding

$$\rho(k;l) = \frac{\sum_{i;j=0}^{47} w^2(i;j)f(i;j)g(i+k;j+l)}{\sqrt{\left(\sum_{i;j=0}^{47} w^2(i;j)f^2(i;j)\right)\left(\sum_{i;j=0}^{47} w^2(i;j)g^2(i+k;j+l)\right)}}$$

$$+\frac{\sum_{i;j=0}^{47} w^2(i;j) f(i-k;j-l) g(i;j)}{\sqrt{\left(\sum_{i;j=0}^{47} w^2(i;j) f^2(i-k;j-l)\right)\left(\sum_{i;j=0}^{47} w^2(i;j) g^2(i;j)\right)}} \tag{5}$$

in the present notation. Compared to the other implementations of the weights, introduced in [30] or [39], the "doubled weighting" is more accurate and has a smaller tendency to yield outliers.

The estimation of the displacement between the two re-sampled images is done by finding the maximum in the correlation plane, and then fitting a two-dimensional Gaussian function to the 3×3 pixel surroundings [40].

5 Results

In all test cases, the root mean square (RMS) error of the displacement estimates has been calculated from a series of 100 pairs of images.

5.1 Test case 1: No interpolation, no truncation

In the first test case, the effect of the varying intensity of particle images is investigated without the influence of weighting schemes, truncation or interpolation errors. Approximately 42 particles (determined by a Poisson random process) have been placed in the 32×32 pixel center part of the 48×48 pixel interrogation area to avoid truncation at the edges of the interrogation window and no weighting has been applied. The overlaying curves for the estimation with and without the normalization in figure 5a indicate that the normalization of the correlation function has no effect on the correlation estimator for identical particle image intensities in the two consecutive images. Since the re-sampling has been performed at the coordinates of the original images, all interpolation schemes exactly reproduce the original images. In the case of a Gaussian low-pass filter the particle images are broadend. The reduced under-sampling of the Gaussian shaped particle images improves the displacement accuracy. The RMS error drops below 0.01 pixels for particle image diameters slightly larger than 2 pixels.

In the case of varying particle image intensities (figure 5b) without interpolation, for small particle images the estimation error is almost the same as before. For larger particle images, the probability of overlaps increases. In combination with the varying intensities, this yields a bias of the individual displacement estimate and, finally, an increasing RMS error of the estimation process. The situation is even worse for the Gaussian filter. Since this filter broadens the particle images, the probability of overlaps is higher. For increased particle image diameters without interpolation as well as for the Gaussian low-pass filter, unfortunately, this error dominates the decreasing estimation error due to the formally observed reduced under-sampling. Furthermore, if the normalization of the correlation estimates is applied, additional outliers can be observed, which can be seen as spikes with high RMS values in figure 5b.

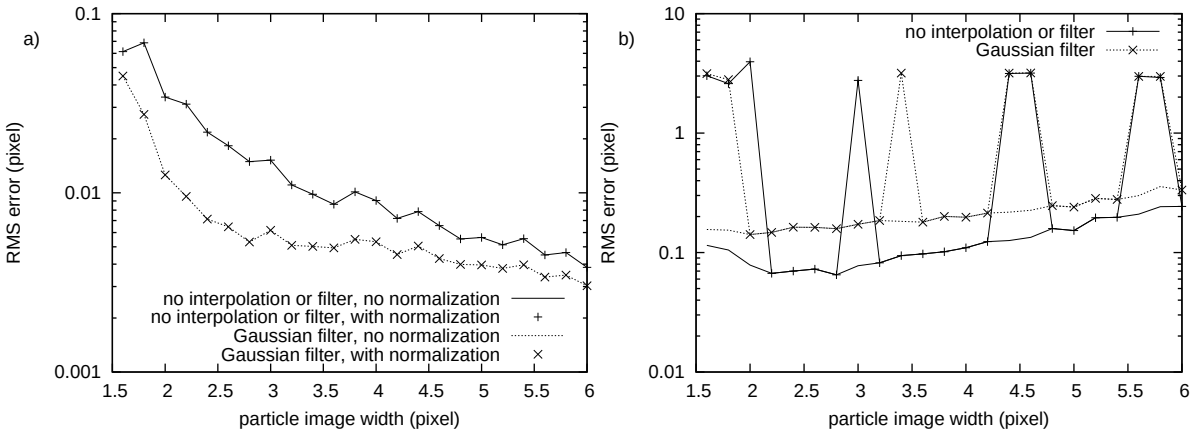

Figure 5: RMS deviation of the displacement estimate for test case 1 (without interpolation or truncation): a) identical particle image intensity in both images and b) intensity variation (lines without symbols: no normalization; lines with symbols: normalization of the correlation function)

5.2 Test case 2: Identical particle image intensity in both images, truncation and interpolation

In the second test case the influence of the interpolation and re-sampling is investigated. To simulate an iterative optimization of the velocity estimate, the re-sampling is done by a symmetric window shift based on either a random pre-estimate or the correct velocity value. The particle images each have random intensities, but the same intensity in both images. They are randomly distributed over the entire interrogation area and its surroundings with approximately 0.04 particles per pixel. Therefore, the particle images are truncated at the edges of the interrogation area. Weighting schemes have not been applied.

For a random pre-estimate of the velocity and without the normalization of the correlation function (lines without symbols in figure 6a), first the RMS error decreases with increasing particle image diameter for all interpolation schemes due to a reduced under-sampling, except for the Gaussian filter. Then the RMS error increases again, due to the dominating influence of a higher probability of truncated particle images at the edges of the interrogation area. Higher-order interpolation schemes like bi-cubic splines or Whittaker perform better than the bi-linear interpolation and have their optimum between 2.5 and 3 pixel particle image diameter. The Gaussian filter increases the probability of truncation, since it broadens the particle image diameter.

The normalization of the correlation function (lines with symbols in figure 6a) significantly reduces the effect of truncated particle images. In this case, for all interpolation schemes the effect of under-sampling dominates in the entire range of particle image diameters, yielding an RMS error which decreases with increasing particle images. For the Whittaker interpolation, the

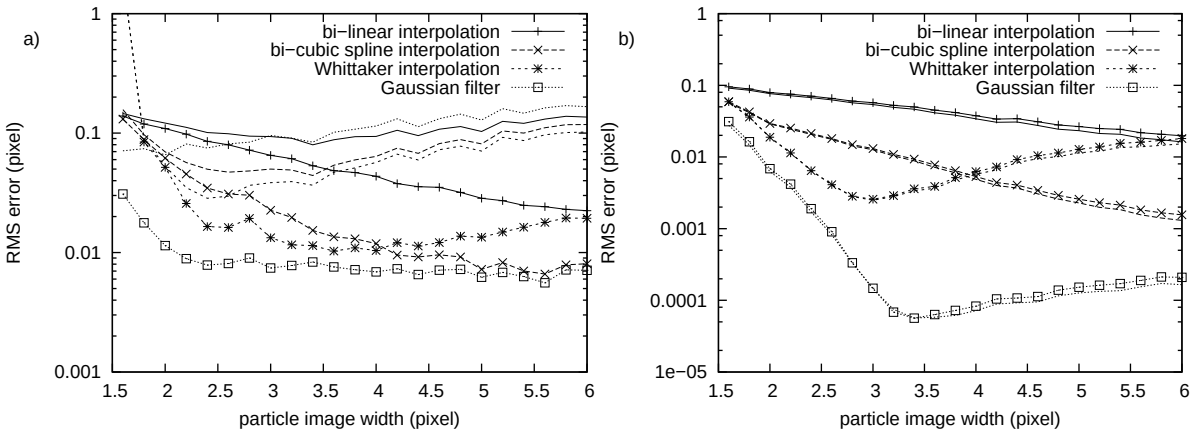

Figure 6: RMS deviation of the displacement estimate for test case 2 (identical particle image intensity in both images, truncation and interpolation): a) image shift based on a random velocity pre-estimate and b) on the correct displacement (lines without symbols: no normalization; lines with symbols: normalization of the correlation function)

RMS error increases for large particle image widths above 4 pixels, which is an effect of the limited interpolation base of 8×8 pixels. Since the under-sampling is significantly reduced by the Gaussian low-pass filter, the positive effect of the normalization is most pronounced for this re-sampling scheme. In the entire range of particle image diameters the results are better than those obtained with any other interpolation scheme. Especially for small particle image diameters, the combination of reduced under-sampling (Gaussian low-pass filter) and corrected truncation (normalization) yields significantly better velocity estimates.

Assuming an iterative optimization of the sub-pixel displacement that converges towards the correct velocity estimate, the remaining RMS error can be reduced further (figure 6b). In this case, the re-sampled images ideally match without any displacement, except for interpolation errors. As before, the particle images are truncated at the edges of the interrogation areas, however, the truncation is identical in both re-sampled images, which then entirely avoids any bias due to the truncation. Therefore, the normalization of the correlation function does not improve the estimation. Even worse, for larger particle image diameters, the estimation with normalization has a slightly larger RMS error than without. In all cases, the Gaussian interpolation yields the best results, which also is limited by the 8×8 pixel interpolation base.

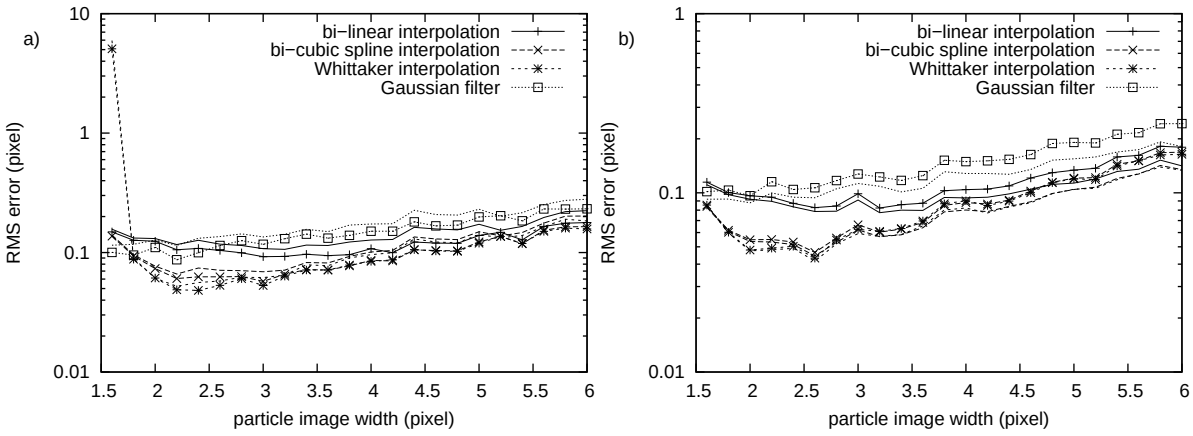

Figure 7: RMS deviation of the displacement estimate for test case 3 (varying particle image intensities, truncation and interpolation): a) image shift based on a random velocity pre-estimate and b) on the correct displacement (lines without symbols: no normalization; lines with symbols: normalization of the correlation function)

5.3 Test case 3: Varying particle image intensities, truncation and interpolation

This picture changes dramatically when varying intensities of the particle images are considered (figure 7). In this case, for all interpolation schemes, including the Gaussian filter, the effect of normalizing the correlation function is minor. It is strongly dominated by the RMS error of the varying particle image intensities in combination with their overlap. In particular, the Gaussian interpolation is very sensitive to this influence due to the broadened particle images and the higher probability of overlaps. The bi-cubic spline and the Whittaker interpolation yield comparable results, which are significantly better than those of the other schemes. In all cases, the normalization slightly reduces the RMS error for random velocity pre-estimates, while it increases the RMS error slightly for the correct velocity pre-estimate.

5.4 Test case 4: Identical particle image intensity in both images, truncation, interpolation and interrogation area weighting

In the following two test cases, interrogation area weighting is also used. Even if usually a larger interrogation area size is used with the weighting to keep the effective window size or the amount of usable image information constant, the size has not changed in this study for comparison.

Due to the non-sharp edges of the weighting function, the influence of truncated particle images without normalization is smaller than without the weight-

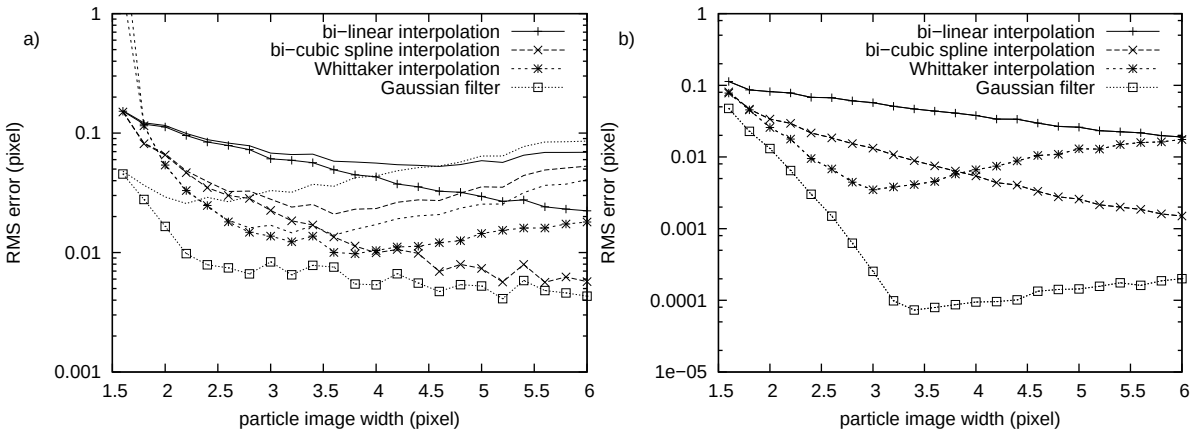

Figure 8: RMS deviation of the displacement estimate for test case 4 (identical particle image intensity in both images, interpolation and interrogation area weighting): a) image shift based on a random velocity pre-estimate and b) on the correct displacement (lines without symbols: no normalization; lines with symbols: normalization of the correlation function)

ing (lines without symbols in figure 8a compared to figure 6a). For large particle images, this yields decreased RMS errors. With normalization (lines with symbols), the results are almost identical to those without weighting. This indicates that the normalization efficiently removes the truncation error.

For a window shift based on the correct velocity (figure 8b), the particle image truncation does not affect the estimation, because the truncation is identical in both images. Therefore, the curves with and without normalization are identical here and very close to the results without weighting in figure 6b. The Gaussian filter is superior in the entire range of particle image diameters.

5.5 Test case 5: Varying particle image intensities, truncation, interpolation and interrogation area weighting

For varying particle image intensities (figure 9) the diagrams have been rearranged. In figure 9a the RMS errors are shown for the estimates without normalization, image shifts based on a random displacement pre-estimate and the correct displacement together. The overlaying curves show clearly that the error due to the varying particle image intensities in combination with their overlap dominates all other errors. The spike in the diagram also shows the increased probability of outliers in this case.

In figure 9b the results are shown for the estimation with normalization. Since the error due to the varying intensities dominates the truncation error, the normalization is not able to reduce the RMS value. On the other hand, the probability of outliers is significantly larger with normalization than without.

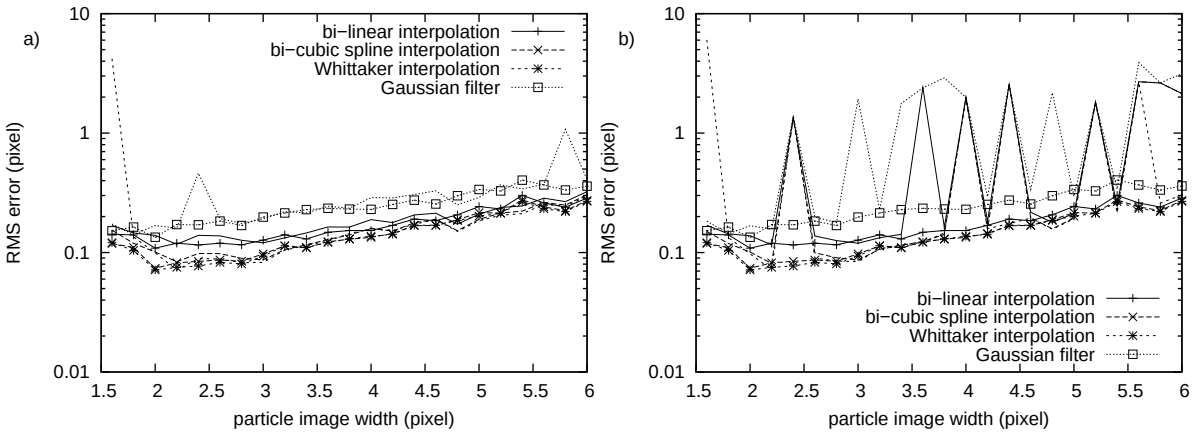

Figure 9: RMS deviation of the displacement estimate for test case 5 (varying particle image intensities, interpolation and interrogation area weighting): a) without normalization and b) with normalization (lines without symbols: image shift based on a random velocity pre-estimate; lines with symbols: image shift based on the correct displacement)

Since the Gaussian filter broadens the particle images and increases the probability of overlaps, the RMS errors of the Gaussian filter are even higher than for the other interpolation schemes in the entire range of particle image diameters. For larger diameters, the results of the other interpolation schemes converge, while for the interesting range of 2 through 3.5 pixels, the bi-cubic spline and the Whittaker interpolation yield comparable results that are both superior to the other interpolations.

Compared to the estimation without weighting (figure 7), the triangular weighting yields slightly larger RMS errors, which indicates a loss of information due to the weighting. Since the RMS error depends on the size of the interrogation area, this can be compensated by increasing the interrogation area size for the weighting scheme. Usually, the dimensions are doubled compared to the non-weighted interrogation area, also to avoid outliers. Even if the application of the weighting scheme has an advanced frequency response and, hence, yields a better resolution, it does not improve the achievable accuracy, which is dominantly limited by the intensity fluctuations.

5.6 Test case 6: Varying particle image intensities, truncation and interpolation

Since the normalization and the interrogation area weighting do not improve the accuracy of the displacement estimation, the last test case investigates the influence of experimental and analysing parameters, namely the particle density and the size of the interrogation areas.

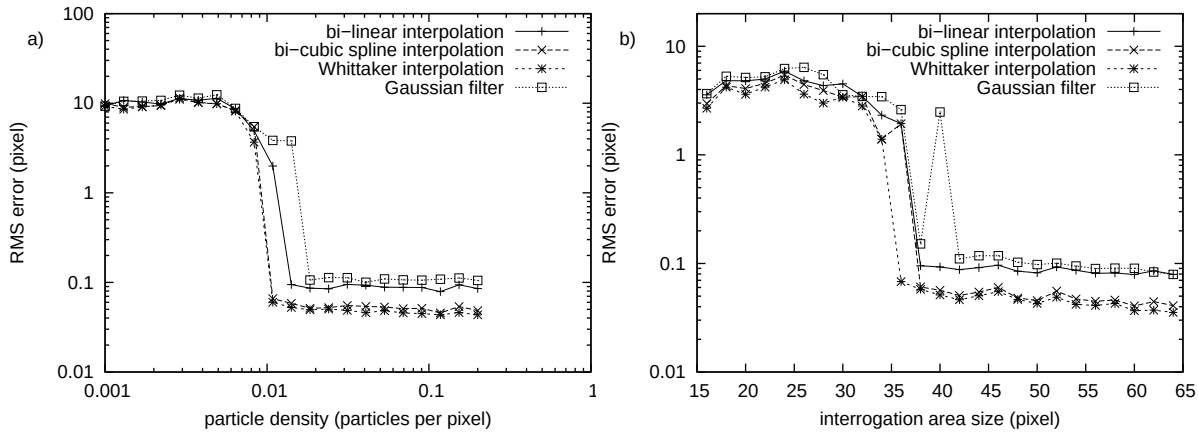

Figure 10: RMS deviation of the displacement estimate for test case 6 (varying particle image intensities, truncation and interpolation): a) influence of the particle density and b) influence of the interrogation area size

In figure 10a the RMS deviation of the displacement estimate is shown as a function of the particle density. The diameter of the particle images is 2.5 pixels and the size of the interrogation area is 48×48 pixels without interrogation area weighting and without the normalization. The re-sampling with the symmetric window shift is based on the correct velocity in this simulation. Since the estimation error is dominated by the fluctuations of the particle image intensity in combination with their overlap, a higher particle density cannot improve the accuracy due to an increasing probability of particle image overlaps. Below a certain particle density, the displacement estimation becomes unrelaiable, generating outliers, which significantly increase the RMS error.

In figure 10b the RMS deviation of the displacement estimate is shown as a function of the interrogation area size. The diameter of the particle images is 2.5 pixels and the particle density is 0.04 particles per pixel, again without interrogation area weighting and without the normalization and with a symmetric window shift based on the correct velocity. Below a certain size of the interrogation areas, the displacement estimation is unreliable and generates outliers. For larger interrogation area sizes, the estimation is reliable with a slightly increasing accuracy for increasing sizes.

In all cases, the reachable accuracy is around 0.1 pixel for the bi-linear interpolation, and slightly worse for the Gaussian filter. Both, the bi-cubic spline and the Whittaker interpolation perform better with a remaining RMS error between 0.04 pixel for large interrogation areas and 0.07 pixel for minimum interrogation areas without outliers.

6 Conclusion

The variation of particle image intensities in the two consecutive images in a PIV measurement limits the obtainable accuracy and increases the probability of outliers. Such intensity variations occur in experiments due to the motion of the particles in the intensity profile of the light sheet or misalignments of the two light pulses.

In the here investigated case of individually varying particle image intensities the normalization of the correlation function is found to be ineffectual. This observation holds, independently of a correct displacement pre-estimate, and the appropriate image re-sampling or the interrogation area weighting. Additionally, it increases the probability of outliers, especially in combination with the application of the weighting scheme.

For large particle image diameters, the error due to the particle intensity variations dominates the error due to the under-sampling of the particle images. This especially affects the results of the Gaussian low-pass filter, while it is almost independent of an interrogation area weighting applied.

In summary, the errors due to the variations of the particle image intensities seriously limits the obtainable accuracy of PIV measurements and could explain the usually observed limit of approximately 0.1 pixel in experiments. Both, the normalization of the correlation function and the Gaussian filter interpolation do not improve the situation and give no added advantage. Best, and among each other comparable results can be obtained using either the bi-cubic spline or the Whittaker interpolation. Interrogation area weighting schemes can be applied to improve the attainable spatial resolution, but have similar limitations in accuracies.

References

[1] T Utami, R F Blackwelder, and T Ueno. A cross-correlation technique for velocity field extraction from particulate visualization. *Exp. in Fluids*, 10:213–223, 1991.

[2] C E Willert and M Gharib. Digital particle image velocimetry. *Exp. in Fluids*, 10:181–193, 1991.

[3] R D Keane and R J Adrian. Theory of cross-correlation analysis of PIV images. *Applied Scientific Research*, 49:191–215, 1992.

[4] J Westerweel. *Digital Particle Image Velocimetry: Theory and Application*. Delft University Press, Delft, The Netherlands, 1993.

[5] F Scarano. Iterative image deformation methods in PIV. *Meas. Sci. Technol.*, 13:R1–R19, 2002.

[6] J S Morgan, D C Slater, J G Timothy, and E B Jenkins. Centroid position measurements and subpixel sensitivity variations with the MAMA detector. *Applied Optics*, 28(6):1178–1192, 1989.

[7] B F Alexander and K C Ng. Elimination of systematic error in sub-pixel accuracy centroid estimation. *Opt. Eng.*, 30:1320–1331, 1991.

[8] A K Prasad, R J Adrian, C C Landreth, and P W Offutt. Effect of resolution on the speed and accuracy of particle image velocimetry interrogation. *Exp. in Fluids*, 13:105–116, 1992.

[9] I Lourenco and A Krothapalli. On the accuracy of velocity and vorticity measurements with PIV. *Exp. in Fluids*, 18:421–428, 1995.

[10] A M Fincham and G R Spedding. Low cost, high resolution DPIV for measurement of turbulent fluid flow. *Exp. in Fluids*, 23:449–462, 1997.

[11] J Westerweel. Effect of sensor geometry on the performance of PIV. In *Proc. 9th Int. Symp. on Appl. of Laser Techn. to Fluid Mechanics*, Lisbon, Portugal, 1998.

[12] K T Christensen. The influence of peak-locking errors on turbulence statistics computed from PIV ensembles. *Exp. in Fluids*, 36:484–497, 2004.

[13] J Nogueira, A Lecuona, and P A Rodriguez. Identification of a new source of peak locking, analysis and its removal in conventional and super-resolution PIV techniques. *Exp. in Fluids*, 30:309–316, 2001.

[14] H T Huang, H E Fiedler, and J J Wang. Limitation and improvement of PIV; part I: Limitation of conventional techniques due to deformation of particle image patterns. *Exp. in Fluids*, 15:263–273, 1993.

[15] H Huang, D Dabiri, and M Gharib. On error of digital particle image velocimetry. *Meas. Sci. Technol.*, 8:1427–1440, 1997.

[16] H Nobach. Accuracy of sub-pixel interpolation in PIV and PTV image processing. Technical report, Technische Universität Darmstadt, Fachbereich Maschinenbau, Fachgebiet Strömungslehre und Aerodynamik, 2004. Report No. 001/2004.

[17] J Nogueira, A Lecuona, and P A Rodriguez. New source of peak locking related to the window size: analysis and its removal. In *Proc. 4rd Int. Symp. on PIV '01*, Göttingen, Germany, 2001. paper 1013.

[18] H Nobach, N Damaschke, and C Tropea. High-precision sub-pixel interpolation in PIV/PTV image processing. In *Proc. 12th Int. Symp. on Appl. of Laser Techn. to Fluid Mechanics*, Lisbon, Portugal, 2004. paper 24.1.

[19] H T Huang, H E Fiedler, and J J Wang. Limitation and improvement of PIV; part II: Particle image distorsion, a novel technique. *Exp. in Fluids*, 15:263–273, 1993.

[20] B Lecordier. *Etude de l'interaction de la propagation d'une flamme premelangee avec le champ aerodynamique, par association de la tomographie Laser et de la Velocimetrie par Images de particules.* PhD thesis, l'Universite de Rouen, 1997.

[21] O T Tokumaru and P E Dimotakis. Image correlation velocimetry. *Exp. in Fluids*, 19:1–15, 1995.

[22] K Jambunathan, X Y Ju, B N Dobbins, and S Ashforth-Frost. An improved cross correlation technique for particle image velocimetry. *Meas. Sci. Technol.*, 6:507–514, 1995.

[23] T Roesgen. Optimal subpixel interpolation in particle image velocimetry. *Exp. in Fluids*, 35:252–256, 2003.

[24] T Astarita and G Cardone. Analysis of interpolation schemes for image deformation methods in piv. *Exp. in Fluids*, 38:233–243, 2005.

[25] J Chen and J Katz. Elimination of peak-locking error in PIV analysis using the correlation mapping method. *Meas. Sci. Technol.*, 16:1605–1618, 2005.

[26] T Astarita. Analysis of interpolation schemes for image deformation methods in piv: effect of noise on the accuracy and spatial resolution. *Exp. in Fluids*, 40:977–987, 2006.

[27] J M Whittaker. The Fourier theory of the cardinal functions. *Proc. - R. Soc. Edinburgh Sect. A Math.*, 1:169–176, 1929.

[28] H Nobach, N Damaschke, and C Tropea. High-precision sub-pixel interpolation in particle image velocimetry image processing. *Experiments in Fluids*, 39:299–304, 2005.

[29] M Stanislas, K Okamoto, and C Kähler. Main results of the first international PIV challenge. *Meas. Sci. Technol.*, 14(10):R63–R89, 2003.

[30] J Nogueira, A Lecuona, and P A Rodriguez. Local field correction PIV: on the increase of accuracy of digital PIV systems. *Exp. in Fluids*, 27:107–116, 1999.

[31] J Nogueira, A Lecuona, and P A Rodríguez. Local field correlation PIV, implementated by means of simple algorithms, and multigrid versions. *Meas. Sci. Technol.*, 12:1911–1921, 2001.

[32] F Scarano. On the stability of iterative PIV image interrogation methods. In *Proc. 12th Int. Symp. on Appl. of Laser Techn. to Fluid Mechanics*, Lisbon, Portugal, 2004.

[33] J Nogueira, A Lecuona, U Ruiz-Rivas, and P A Rodríguez. Analysis and alternatives in two-dimensional multigrid particle image velocimetry methods: application of a dedicated weighting function and symmetric direct correlation. *Meas. Sci. Technol.*, 13:963–974, 2002.

[34] A Lecuona, J Nogueira, P A Rodríguez, and D Santana. Accuracy and time performance of different schemes of the local field correlation technique. *Exp. in Fluids*, 33:743–751, 2002.

[35] B Lecordier and M Trinité. Accuracy assessment of image interpolation schemes for PIV from real images of particle. In *Proc. 13th Int. Symp. on Appl. of Laser Techn. to Fluid Mechanics*, Lisbon, Portugal, 2006. paper 26.4.

[36] R D Keane and R J Adrian. Optimization of particle image velocimeters. part i: Double pulsed systems. *Meas. Sci. Technol.*, 1:1202–1215, 1990.

[37] R D Keane, R J Adrian, and Y Zhang. Super-resolution particle image velocimetry. *Meas. Sci. Technol.*, 6:754–768, 1995.

[38] J Westerweel. Theoretical analysis of the measurement precision in particle image velocimetry. *Exp. in Fluids*, 29:S3–S12, 2000.

[39] H Nobach and C Tropea. Improvements to PIV image analysis by recognizing the velocity gradients. *Experiments in Fluids*, 39:612–620, 2005.

[40] H Nobach and M Honkanen. Two-dimensional Gaussian regression for sub-pixel displacement estimation in particle image velocimetry or particle position estimation in particle tracking velocimetry. *Experiments in Fluids*, 38:511–515, 2005.